Journal of Computational Physics 488 (2023) 112169

Contents lists available at ScienceDirect

Journal of Computational Physics

journal homepage: www.elsevier.com/locate/jcp

Residual distribution schemes for steady radiative transfer equations on unstructured meshes

Jiexing Zhang [a], Qingjie Cui [a], Yibing Chen [b], Guoxi Ni [b,*]

[a] Graduate school of China Academy of Engineering Physics, Beijing, China
[b] Institute of Applied Physics and Computational Mathematics, Beijing, China

ARTICLE INFO

Article history:
Received 14 June 2022
Received in revised form 9 April 2023
Accepted 17 April 2023
Available online 3 May 2023

Keywords:
Residual distribution
Radiative transfer
Steady state
Conservative
Unstructured meshes

ABSTRACT

We consider the numerical solution of steady radiative transfer equations on unstructured meshes. The radiative transfer equations belong to a class of integro-differential equations. We apply conservative residual distribution (RD) methods to solve the radiative transfer equations. To achieve this, we first adopt the discrete ordinate method for angular discretization and use the RD methods to solve the resulting system of coupled linear hyperbolic equations. We present some basics and accuracy analysis for the RD schemes. The standard nonlinear limiter is adopted to upgrade the monotonicity preserving first-order scheme for a high-order one. Several numerical experiments show that the proposed RD schemes achieve second-order accuracy and verify the non-oscillatory property of our numerical schemes.

1. Introduction

The radiative transfer equation (RTE) describes photon propagation in participating media taking into account the dynamics of its transport and collision with material, it has wide applications in various areas such as heat transfer, atmospheric radiative transfer, inertial confinement fusion, optical imaging, astrophysics, and so on.

Mathematically, the radiative transfer equation is an integro-differential equation with the spatial, the directional coordinates and a time variable. In general, it is almost impossible to obtain an analytical solution on account of the mathematical complexity and complex configuration of practical problems, thus numerical simulation becomes a practical tool to analyze the radiative transfer process. However, due to the high dimensionality and the presence of integral coupling terms, it brings challenges for developing effective and accurate numerical methods for solving the RTEs.

The existing numerical methods for solving the RTEs can be roughly classified into two types: the first one is based on stochastic simulation such as Monte Carlo method [1,2]; the other one is the deterministic method based directly on the integro-differential equation, such as spherical harmonics method [3], discrete ordinate method (DOM) [4], finite volume method (FVM) [5], finite element method (FEM) [6], discontinuous Galerkin (DG) method [7–9], spectral method [10], and gas kinetic schemes [11–13]. The readers can refer to [14] for a detailed review of numerical methods for the RTEs. In addition, it is usually required to have some special design principles in order to maintain some physical properties of the solution. For example, when there occurs diffusive radiative behavior due to severe interaction between radiation and material, one has to consider the asymptotic preserving behavior of numerical schemes. For angular discretization, the idea

* Corresponding author.
E-mail address: gxni@iapcm.ac.cn (G. Ni).

https://doi.org/10.1016/j.jcp.2023.112169
0021-9991/

of DOM is to discretize the angular space into finite discrete directions and solve the radiative intensity only in these discrete directions. Due to its relatively high accuracy and operability, DOM is widely applied to the numerical solution of transport equations. After the angular discretization, the original integro-differential form of RTE becomes a system of linear hyperbolic equations coupled with source terms.

In recent years, residual distribution (RD) methods have been developed systematically for these types of linear and nonlinear hyperbolic equations. It can be traced back to the Lax-Wendroff residual distribution scheme [15] proposed by R.-H. Ni and the residual distribution framework [16] proposed by P.L. Roe, which has caught the interest of researchers due to the possibility of constructing multidimensional upwind schemes. In general, RD methods possess several advantages such as conservation property, high-order accuracy, and less sensitivity to mesh variations, see [17]. RD methods have been applied in numerical simulations for different problems. In [18–20], conservative RD methods are proposed for advection problems including the Euler equations, then have been extended for advection-diffusion problems in [21–23], and the shallow water equations in [24,25]. High-order RD methods have been studied for steady problems in [26–28], and for unsteady cases in [29,30]. These series of research results enrich the framework of RD methods and verify some great advantages of RD schemes.

In this paper, we are interested in constructing conservative RD schemes for steady RTEs. Due to the property of photons and the presence of angular integral term and external source term, it brings some extra difficulties to generalize existing RD methods for the RTEs. Some representative work associated with the discretization of source terms in advection equations is worth mentioning here. In [25,31] Ricchiuto et al. propose RD methods with well balanced source terms for the shallow water equations, and Abgrall et al. propose high-order RD methods for kinetic models with stiff source terms in which the sources are discretized implicitly with a Galerkin residual [32]. A more general treatment of source terms has been heuristically discussed in [33].

To deal with the scattering integral term in the RTE, we first adopt the DOM to discretize the angular space, then obtain the system of coupled hyperbolic equations, which could be solved with RD methods. The classical RD schemes such as the N scheme can be used to discretize the transport term of RTE, while the other parts including the absorbing-scattering and source term should be discretized consistently, which guarantees consistency and accuracy of the overall schemes. To achieve this, we consider the variational formulation of RD schemes, in which RD schemes can be carried out in the finite element frame, then construct a consistent test function for the discretization of sources. Moreover, we adopt a standard nonlinear mapping to upgrade the accuracy to high-order while maintaining the monotonicity preserving property of RD schemes [34,35], in which the key ingredient is to construct positive coefficients in the residuals. To achieve monotonicity preserving property, there exist some limiting techniques used in finite element approximation, such as [36–38] and references therein. We should stress that monotonicity preserving property is essential to the simulation of advection problems, especially at discontinuities occurring in the solution.

The structure of the paper is as follows. In Section 2, we start by introducing the radiative transfer equations, followed by the discretization of the angular space. In Section 3, we recall some basics of RD schemes and analyze the accuracy of RD schemes in the presence of source terms. Next, we present the standard technique to upgrade the monotonicity preserving low-order schemes to high-order ones and extend the RD methods to solve steady RTEs by constructing a consistent test function in the variational formulation. In Section 4, the proposed RD schemes are extensively tested on various numerical problems which verify the accuracy and robustness of our schemes. Finally, we make some concluding remarks in Section 5.

2. The radiative transfer equations and the angular discretization

We recall the radiative transfer equations and introduce the angular discretization by using the DOM, which is a basic step in our numerical schemes.

2.1. The radiative transfer equations

The radiative transfer equation is the mathematical statement of the conservation of photons [39]. We consider a one-group, isotropically scattering transfer equation as follows,

$$\frac{1}{c}\frac{\partial I(\boldsymbol{r},\boldsymbol{\Omega},t)}{\partial t}+\boldsymbol{\Omega}\cdot\nabla I(\boldsymbol{r},\boldsymbol{\Omega},t)+\sigma_t I(\boldsymbol{r},\boldsymbol{\Omega},t)=\frac{\sigma_s}{4\pi}\int_S I(\boldsymbol{r},\boldsymbol{\Omega}',t)\mathrm{d}\boldsymbol{\Omega}'+q(\boldsymbol{r},\boldsymbol{\Omega},t), \tag{1}$$

where c is the speed of photon, $I(\boldsymbol{r},\boldsymbol{\Omega},t)$ is the radiative intensity in the direction $\boldsymbol{\Omega}$, at the spatial position $\boldsymbol{r}$ and at the time t, S is the unit sphere, $\sigma_s\geq 0$ is the scattering coefficient of the medium, $\sigma_t\geq\sigma_s$ is the extinction coefficient of the medium due to both absorption and scattering, and $q(\boldsymbol{r},\boldsymbol{\Omega},t)$ is a given source term. The vector $\boldsymbol{r}$ denotes the spatial position in the Cartesian coordinate system, and the vector $\boldsymbol{\Omega}$ denotes the unit vector of the direction of motion of the particle, also called the solid angle, which is determined by a polar angle θ and a corresponding azimuthal angle φ in the polar coordinate system, and total solid angle is 4π spherical degree.

To further simplify the RTE above, we introduce $\mu=\cos\theta$, $\zeta=\sin\theta\cos\varphi$, $\eta=\sin\theta\sin\varphi$, then

$$\mathrm{d}\boldsymbol{\Omega}=\sin\theta\mathrm{d}\theta\mathrm{d}\varphi=-\mathrm{d}\mu\mathrm{d}\varphi,$$

thus the scattering integral term can be rephrased as

$$\int_S I(\boldsymbol{r}, \boldsymbol{\Omega}, t)\mathrm{d}\boldsymbol{\Omega} = \int_0^{2\pi}\int_0^{\pi} I(\boldsymbol{r}, \theta, \varphi, t)\sin\theta \mathrm{d}\theta\mathrm{d}\varphi = \int_0^{2\pi}\int_{-1}^{1} I(\boldsymbol{r}, \mu, \varphi, t)\mathrm{d}\mu\mathrm{d}\varphi.$$

We notice that $\boldsymbol{\Omega}\cdot\nabla I(\boldsymbol{r}, \boldsymbol{\Omega})$ could be interpreted as a directional derivative in the $\boldsymbol{\Omega}$ direction. That is, we write

$$\boldsymbol{\Omega}\cdot\nabla I = \lim_{\Delta s\to 0}\frac{I(\boldsymbol{r}+\Delta s\boldsymbol{\Omega}, \boldsymbol{\Omega}) - I(\boldsymbol{r}, \boldsymbol{\Omega})}{\Delta s} = \frac{\mathrm{d}I}{\mathrm{d}s},$$

where s is a length along $\boldsymbol{\Omega}$.

When we consider the steady problem, the time derivative term vanishes, i.e. $\frac{\partial I}{\partial t} = 0$, then we derive the mathematical forms of the one- and two-dimensional steady radiative transfer equations.

In the one-dimensional (1D) case, the radiative intensity I only depends on the spatial coordinate z and the angular coordinate θ. The directional derivative can be expressed as follows

$$\boldsymbol{\Omega}\cdot\nabla I(\boldsymbol{r}, \boldsymbol{\Omega}) = \frac{\mathrm{d}I}{\mathrm{d}s} = \frac{\partial I}{\partial z}\frac{\mathrm{d}z}{\mathrm{d}s} = \mu\frac{\partial I}{\partial z},$$

and the scattering integral term can be rewritten as

$$\frac{1}{4\pi}\int_S I(\boldsymbol{r}, \boldsymbol{\Omega})\mathrm{d}\boldsymbol{\Omega} = \frac{1}{4\pi}\int_0^{2\pi}\int_{-1}^{1} I(z, \mu)\mathrm{d}\mu\mathrm{d}\varphi = \frac{1}{2}\int_{-1}^{1} I(z, \mu)\mathrm{d}\mu.$$

Thus we obtain the 1D steady radiative transfer equation

$$\mu\frac{\partial I(z, \mu)}{\partial z} + \sigma_t I(z, \mu) = \frac{\sigma_s}{2}\int_{-1}^{1} I(z, \mu)\mathrm{d}\mu + q(z, \mu). \tag{2}$$

In the two-dimensional (2D) case, the radiative intensity I depends on the spatial coordinate x and y and the angular coordinate θ and φ. Similarly, we derive the directional derivate as

$$\boldsymbol{\Omega}\cdot\nabla I(\boldsymbol{r}, \boldsymbol{\Omega}) = \frac{\mathrm{d}I}{\mathrm{d}s} = \zeta\frac{\partial I}{\partial x} + \eta\frac{\partial I}{\partial y},$$

and the scattering integral term given by

$$\frac{1}{4\pi}\int_S I(\boldsymbol{r}, \boldsymbol{\Omega})\mathrm{d}\boldsymbol{\Omega} = \frac{1}{4\pi}\int_0^{2\pi}\int_{-1}^{1} I(x, y, \sqrt{1-\mu^2}\cos\varphi, \sqrt{1-\mu^2}\sin\varphi)\mathrm{d}\mu\mathrm{d}\varphi.$$

Thus we obtain the 2D steady radiative transfer equation

$$\zeta\frac{\partial I(x, y, \zeta, \eta)}{\partial x} + \eta\frac{\partial I(x, y, \zeta, \eta)}{\partial y} + \sigma_t I(x, y, \zeta, \eta) = \frac{\sigma_s}{4\pi}\int_0^{2\pi}\int_{-1}^{1} I(x, y, \zeta, \eta)\mathrm{d}\mu\mathrm{d}\varphi + q(x, y, \zeta, \eta), \tag{3}$$

where $\zeta = \sqrt{1-\mu^2}\cos\varphi$, $\eta = \sqrt{1-\mu^2}\sin\varphi$.

2.2. The angular discretization

To solve the radiative transfer equation (2) and (3) numerically, we have to discretize the equation in both spatial and angular spaces. We first adopt the discrete ordinate method to discretize the angular variable $\boldsymbol{\Omega}$ into a finite number of directions spanning the total solid angles of the unit sphere around a point in space, then obtain a system of linear hyperbolic equations coupled with source terms. Then we use the RD method to calculate the radiative intensity in each discrete direction.

Consider a steady radiative transfer equation on the domain $\mathbb{D}\subseteq\mathbb{R}^d$ $(d = 1, 2)$

$$\boldsymbol{\Omega}\cdot\nabla I(\boldsymbol{r}, \boldsymbol{\Omega}) + \sigma_t I(\boldsymbol{r}, \boldsymbol{\Omega}) = \frac{\sigma_s}{4\pi}\int_S I(\boldsymbol{r}, \boldsymbol{\Omega}')\mathrm{d}\boldsymbol{\Omega}' + q(\boldsymbol{r}, \boldsymbol{\Omega}), \quad \boldsymbol{r}\in\mathbb{D}, \tag{4}$$

where $\partial\mathbb{D}$ denotes the domain boundary. We define $\partial\mathbb{D}_{\text{in}} = \{\boldsymbol{r} | \boldsymbol{r} \in \partial\mathbb{D}, \boldsymbol{n}(\boldsymbol{r}) \cdot \boldsymbol{\Omega} < 0\}$, where $\boldsymbol{n}(\boldsymbol{r})$ denotes the unit outward normal vector at the point $\boldsymbol{r}$ on $\partial\mathbb{D}$. We impose the inflow boundary condition

$$I(\boldsymbol{r}, \boldsymbol{\Omega}) = g(\boldsymbol{r}, \boldsymbol{\Omega}), \quad \boldsymbol{r} \in \partial\mathbb{D}_{\text{in}}, \tag{5}$$

where g is a given function.

For each discrete direction $\boldsymbol{\Omega}^m$, $m = 1, \ldots, M$, the equation (4) can be written as a set of linear hyperbolic equations

$$\boldsymbol{\Omega}^m \cdot \nabla I^m(\boldsymbol{r}) + \sigma_t I^m(\boldsymbol{r}) = \sigma_s \sum_{m'=1}^{M} \omega^{m'} I^{m'}(\boldsymbol{r}) + q^m(\boldsymbol{r}), \quad m = 1, \ldots, M, \tag{6}$$

where $I^m(\boldsymbol{r}) = I(\boldsymbol{r}, \boldsymbol{\Omega}^m)$, $q^m(\boldsymbol{r}) = q(\boldsymbol{r}, \boldsymbol{\Omega}^m)$ and the integral $\frac{1}{4\pi}\int_S I(\boldsymbol{r}, \boldsymbol{\Omega}')\mathrm{d}\boldsymbol{\Omega}'$ is approximated by the Legendre-Chebyshev P_N-T_N quadrature formula $\sum_{m'=1}^{M} \omega^{m'} I^{m'}(\boldsymbol{r})$, that is,

$$\frac{1}{4\pi}\int_S I(\boldsymbol{r}, \boldsymbol{\Omega}')\mathrm{d}\boldsymbol{\Omega}' \approx \sum_{m'=1}^{M} \omega^{m'} I^{m'}(\boldsymbol{r}),$$

with the quadrature weights satisfying

$$\sum_{m'=1}^{M} \omega^{m'} = 1 \quad \text{and} \quad \omega^{m'} > 0.$$

The remaining work is to solve every hyperbolic equation (6) in the corresponding discrete direction.

3. Conservative residual distribution schemes

In this section, we present our residual distribution schemes for the system of equations (6), in which each one is a linear hyperbolic equation in each discrete direction. We begin with a monotonicity preserving RD scheme and upgrade it to be a second-order one for solving the RTE with general sources.

3.1. Basic formulation

Let us first introduce some notations used for the mesh and related geometrical entities. The computational domain $\mathbb{D}$ is covered by a tessellation $\mathcal{T}_h$. In this paper, the mesh is assumed to be shape regular and composed of triangles in $\mathbb{R}^2$. We denote by E the generic element and by h_E the diameter of the element E. A global mesh size is given by $h = \max_{E\in\mathcal{T}_h} h_E$.

We consider a general form of the RTE (6) after the angular discretization as follows

$$\boldsymbol{\Omega}^m \cdot \nabla I^m(\boldsymbol{r}) = S^m(I^m, \boldsymbol{r}), \quad m = 1, \ldots, M, \tag{7}$$

where $S^m(I^m, \boldsymbol{r})$ contains the absorption-scattering term and source term, that is,

$$S^m(I^m, \boldsymbol{r}) = -\sigma_t I^m(\boldsymbol{r}) + \sigma_s \sum_{m'=1}^{M} \omega^{m'} I^{m'}(\boldsymbol{r}) + q^m(\boldsymbol{r}).$$

Taking account of the equivalence in coping with the RTE in each discrete direction $\boldsymbol{\Omega}^m$, here we omit the superscript m of these quantities associated with the discrete direction $\boldsymbol{\Omega}^m$ for simplicity, i.e. we would use I, S corresponding to I^m, S^m, unless otherwise stated.

In the RD schemes, the unknowns are discretized in a finite element space $\mathcal{V}_h$ associated with the computational mesh, and the discrete unknowns are a set of local values of the solution in some mesh locations, such as the vertices M_i, edge mid-points, etc. The unknown function is defined by the set of local values at all the degrees of freedom (DoFs). If we denote by $\mathcal{S}$ the set of degrees of freedom, we have

$$I_h(\boldsymbol{r}) = \sum_{i\in\mathcal{S}} I_i \psi_i(\boldsymbol{r}),$$

where I_h is the interpolant of I, and $\psi_i(\boldsymbol{r})$ denotes the basis function whose collection spans the finite element space $\mathcal{V}_h$, i.e. $\mathcal{V}_h = \text{span}\{\psi_i, i \in \mathcal{S}\}$. Considering a second-order RD scheme, the DoFs are at the vertices of the mesh and the interpolant function I_h is assumed to be linear on each element E. When we adopt the Lagrange basis function, the local value of the function I is the nodal value at each DoF, that is $I_i = I_h(M_i)$.

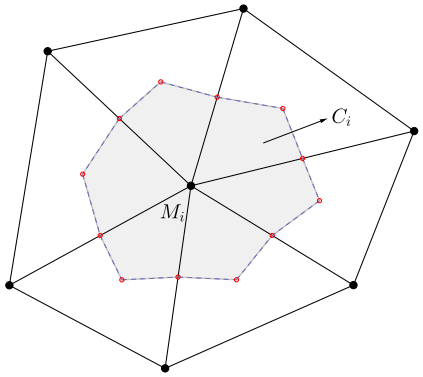

Fig. 1. Median dual cell C_i.

In order to discretize each RTE (7), we consider the following residual distribution scheme:

$$|C_i|\frac{I_i^{(\ell+1)}-I_i^{(\ell)}}{\Delta t}+\sum_{E\ni i}\phi_i^E=0, \tag{8}$$

where $|C_i|$ denotes the area of the dual cell associated with vertex M_i as shown in Fig. 1, Δt is a scaled pseudotime step, $I_i^{(\ell)}$ denotes the value of I at the DoF i and the pseudotime layer ℓ. We stress that the RD scheme would be adopted to solve each single equation in (7), and the superscript m has also been omitted for some related quantities, such as $I_i^{(\ell)}$, ϕ_i^E.

For each equation in (7), we define the total residual on each element E

$$\Phi_E=\int_E \boldsymbol{\Omega}\cdot\nabla I_h(\boldsymbol{r})-S_h(I_h,\boldsymbol{r})\mathrm{d}\boldsymbol{r},$$

we also define ϕ_i^E as the fraction of the element residual Φ_E associated with the vertex M_i, such that the following conservation property is satisfied

$$\sum_{i\in E}\phi_i^E=\Phi_E. \tag{9}$$

If M_i lies on the inflow boundary $\partial\mathbb{D}_{\text{in}}$, we have to take account of the boundary conditions. Let Γ be an inflow edge, we consider a numerical flux $\mathcal{F}$, then we could define boundary residual ϕ_i^Γ which satisfies a conservation property

$$\sum_{i\in\Gamma}\phi_i^\Gamma=\Phi_\Gamma=\int_\Gamma(\mathcal{F}(I_h,g,\boldsymbol{n})-f_h(I_h)\cdot\boldsymbol{n})\,\mathrm{d}s,$$

with flux $f_h=I_h\boldsymbol{\Omega}$. This is equivalent to imposing the boundary condition in the weak sense, which is mostly used for systems of equations, such as the Euler equations. In the scalar case, we could simply impose given nodal values on the inflow boundary.

During the iteration process, the nodal values of the solution are updated by the nonzero total residuals on the elements; when iteration time $\ell\to\infty$ the total residual on each element vanishes, and the steady state solution is obtained.

3.2. Accuracy analysis

We next consider the accuracy of RD methods, and some detailed analysis has been presented in [40]. We would introduce a general definition of a k-th order accurate RD scheme rather than a second-order case that we focus on, which supplies a guideline for designing high-order RD schemes.

For any smooth compactly supported function v, we introduce the following truncation error

$$\mathcal{E}(I_h)=\sum_{i\in\mathcal{T}_h}v_i\left(\sum_{E\ni i}\phi_i^E(I_h)\right). \tag{10}$$

Performing some basic calculations, we derive the truncation error estimate of RD schemes, which is summarized in the following proposition.

Proposition 3.1. *Considering the steady problem (7), given a mesh $\mathcal{T}_h$ satisfying the regularity assumption, let I_h be the $k-1$ degree, k-th order accurate continuous piecewise polynomial interpolant of I, and S_h k-th order accurate approximation of S on $\mathcal{T}_h$, then a RD scheme verifies the truncation error estimate*

$$|\mathcal{E}(I_h)| = \left| \sum_{i\in\mathcal{T}_h} v_i \left(\sum_{E\ni i} \phi_i^E(I_h) \right) \right| \le Ch^k, \tag{11}$$

with C a positive constant which depends on v, I and $\mathcal{T}_h$, provided that

$$\phi_i^E = \mathcal{O}(h^{k+d-1}). \tag{12}$$

For a more detailed derivation of the Proposition 3.1, one can refer to the Sec. 3.2 in [40].

If a RD scheme satisfies the estimate (11), the RD scheme is k-th order accurate. In fact, this conclusion supplies a necessary condition for constructing high-order RD schemes.

Remark 3.1. The truncation error estimate above shows the formal accuracy of the RD scheme, but in no way guarantees that the scheme actually does converge with rate k.

Under the assumption of the Proposition 3.1, indeed we have $\Phi_E = \mathcal{O}(h^{k+d-1})$. Thus, provided that there exist uniformly bounded constants β_i^E such that

$$\phi_i^E = \beta_i^E \Phi_E, \tag{13}$$

then the condition (12) would be satisfied. A RD scheme with uniformly bounded distribution coefficients β_i^E is referred to as linearity preserving ($\mathcal{LP}$). The $\mathcal{LP}$ property supplies an intuitive design criterion for high-order RD schemes, refer to [26,27].

3.3. Mononicity preservation

In this paragraph, we consider the issue of guaranteeing the non-oscillatory character of the numerical solution. We recall the monotonicity preserving scheme which has positive coefficients to yield solutions that verify a discrete maximum principle (DMP). We introduce monotonicity preserving RD schemes for a homogeneous case of (7), that is, $S = 0$.

Considering the RD scheme of the following form

$$\phi_i^E = \sum_{j\in E} c_{ij}(I_i - I_j)$$

where in general the coefficients c_{ij} may depend on the solution, then the pseudotime iteration (8) can be written as

$$I_i^{(\ell+1)} = I_i^{(\ell)} - \left(\frac{\Delta t}{|C_i|} \sum_{E\ni i} \sum_{j\in E} c_{ij}(I_i - I_j) \right)^{(\ell)} = \left(1 - \frac{\Delta t}{|C_i|} \sum_{E\ni i} \sum_{j\in E} c_{ij} \right) I_i^{(\ell)} + \frac{\Delta t}{|C_i|} \sum_{E\ni i} \sum_{j\in E, j\neq i} c_{ij} I_j^{(\ell)}.$$

We can verify the RD scheme is monotonicity preserving provided that $c_{ij} \ge 0$ under the CFL-like condition

$$\Delta t \left[\frac{\sum_{E\ni i} \sum_{j\in E} c_{ij}}{|C_i|} \right] \le 1. \tag{14}$$

One important property of monotonicity preserving schemes exists in that the solution satisfies the discrete maximum principle

$$\min_{E\ni i} \min_{j\in E} I_j^{(0)} \le I_i^{(\ell)} \le \max_{E\ni i} \max_{j\in E} I_j^{(0)}, \tag{15}$$

where $I_j^{(0)}$ denotes the initial value in the DoF location j. The DMP ensures the L^∞ stability of numerical schemes.

Here we introduce two examples of monotonicity preserving RD schemes, which would be used in the numerical experiments later. In a homogeneous case, the element residual is calculated as

$$\Phi_E = \int_E \mathbf{\Omega} \cdot \nabla I_h \mathrm{d}\boldsymbol{r} = \sum_{i\in E} k_i I_i, \tag{16}$$

where

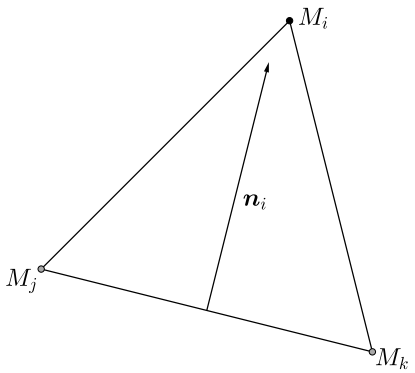

Fig. 2. Inward normal vector $\boldsymbol{n}_i$.

$$k_i = \int_E \boldsymbol{\Omega} \cdot \nabla \psi_i \mathrm{d}\boldsymbol{r} = \frac{1}{2}\boldsymbol{\Omega} \cdot \boldsymbol{n}_i,$$

where $\boldsymbol{n}_i$ denotes the inward pointing vector normal to the edge of E opposite to vertex M_i, scaled by the length of the edge, see Fig. 2.

We recall the N scheme and Lax-Friedrichs scheme, which are well-known as monotonicity preserving first-order RD schemes.

- N scheme

  $$\phi_i^E = k_i^+(I_i - \tilde{I}),$$

  where $x^+ = \max(0, x)$, $x^- = \min(0, x)$. Owing to the conservation property (9) and (16), we obtain

  $$\tilde{I} = \left(\sum_{j\in E} k_J^-\right)^{-1} \left(\sum_{j\in E} k_j^- I_j\right),$$

  where we have used $\sum_{i\in E} k_i = 0$, since $\sum_{i\in E} \boldsymbol{n}_i = 0$. If we define

  $$\lambda = \left(\sum_{j\in E} k_j^-\right)^{-1} \le 0,$$

  then the N scheme can be rewritten as

  $$\phi_i^E = \sum_{j\in E} k_i^+ \lambda k_j^- (I_i - I_j),$$

  where $c_{ij} = k_i^+ \lambda k_j^- \ge 0$, thus the N scheme is monotonicity preserving under the CFL-like condition (14).
- (local) Lax-Friedrichs scheme

  $$\phi_i^E = \frac{1}{N_E}\Phi_E + \alpha(I_i - \bar{I}^E),$$

  where $\bar{I}^E = \frac{1}{N_E}\left(\sum_{j\in E} I_j\right)$ is the arithmetic average of the I_j for $j \in E$, and $\alpha > 0$ is a positive parameter. It is easy to verify that the Lax-Friedrichs scheme is monotonicity preserving provided that

  $$\alpha \ge \max_{j\in E} |k_j|.$$

It is well known that there exists no linear scheme which is monotonicity preserving and has second-order accuracy, owing to the Godunov theorem. Even though we could construct some monotonicity preserving RD schemes, the accuracy of these schemes constructed directly is usually no more than first-order. In the RD framework, some nonlinear mappings would be generally adopted to construct high-order monotonicity preserving RD schemes from low-order ones. We begin with a monotonicity preserving first-order scheme in which residuals are (for $S = 0$)

$$\phi_i^L = \sum_{j\in E} c_{ij}^L (I_i - I_j),$$

here we use superscript L to denote the low-order, and superscript H to denote the high-order later. By assumption, the coefficients c_{ij}^L are all positive, and the conservation relation (9) is satisfied, then let ϕ_i^H denote high-order residuals satisfying that

$$\phi_i^H = \beta_i^H \Phi_E, \quad \sum_{i\in E} \beta_i^H = 1.$$

By analogy, we introduce the distribution coefficients x_i defined by

$$x_i^L = \frac{\phi_i^L}{\Phi_E},$$

for which, we also have $\sum_{i\in E} x_i^L = 1$. We could rewrite the high-order residuals formally as

$$\phi_i^H = \frac{\phi_i^H}{\phi_i^L}\phi_i^L = \sum_{j\in E} \frac{\phi_i^H}{\phi_i^L} c_{ij}^L (I_i - I_j),$$

thus we can construct a monotonicity preserving high-order scheme from the low-order one ϕ_i^L provided that

$$\frac{\phi_i^H}{\phi_i^L} \geq 0, \quad \forall i \in E.$$

For the high-order scheme, thus we have

$$c_{ij}^H = \frac{\phi_i^H}{\phi_i^L} c_{ij}^L \geq 0.$$

These conditions can also be rephrased in terms of x_i^Ls and β_i^Hs, which requires

i. Conservation,

$$\sum_{i\in E} x_i^L = 1, \quad \sum_{i\in E} \beta_i^H = 1.$$

ii. Monotonicity preserving,

$$x_i^L \beta_i^H \geq 0, \quad i \in E.$$

iii. Linearity preserving,

β_i^H is uniformly bounded for any $i \in E$.

The above relations can be interpreted geometrically. For the sake of simplicity, we take an example of the triangular element, i.e. $N_E = 3$, but the extension to other types of elements is also straightforward. It is remarkable to notice that we can interpret the coordinates (x_1, x_2, x_3) (omitting superscript L) and $(\beta_1, \beta_2, \beta_3)$ (omitting superscript H) as the barycentric coordinates of points L and H with respect to an abstract reference triangle (A_1, A_2, A_3), since $\sum_{i\in E} x_i = 1$ and $\sum_{i\in E} \beta_i = 1$. The points L and H are defined by

$$L = x_1 A_1 + x_2 A_2 + x_3 A_3, \quad H = \beta_1 A_1 + \beta_2 A_2 + \beta_3 A_3.$$

In Fig. 3(a), we have divided the whole space into seven sub-domains according to the sign of the barycentric coordinate components: the triangle (A_1, A_2, A_3) and six domains D_i. For example, within the triangle (A_1, A_2, A_3), we have $x_i \geq 0, i = 1, 2, 3$. The key to the problem is to define a mapping that projects the point L onto a bounded subdomain so that points L and H belong to the same subdomain. A geometrical illustration of a possible mapping is shown in Fig. 3(b). We define an invariant region which is bounded, then project onto the invariant region: if the point L lies on the invariant region, the mapping is an identity mapping, i.e. $H = L$; if L lies outside of the invariant region, the mapping projects L to a point H at the boundary of invariant region. We should stress that the mapping satisfies the three constraints. We clarify each β_i is uniformly bounded owing to the boundness of the invariant region. Moreover, the mapping does not change the sign of the barycentric coordinate components, that is, $x_i \beta_i \geq 0$. In practice, the definition of invariant region could be not unique, for example, the dashed circle or the triangle (A_1, A_2, A_3). In Fig. 3(b), a mapping is in detail illustrated that projects the point L on subdomains D_i onto the invariant region, the triangle (A_1, A_2, A_3).

Here we adopt the PSI limiter introduced by R. Struijs in [34], which is corresponding to the nonlinear mapping with invariant region as triangle (A_1, A_2, A_3) in Fig. 3(b)

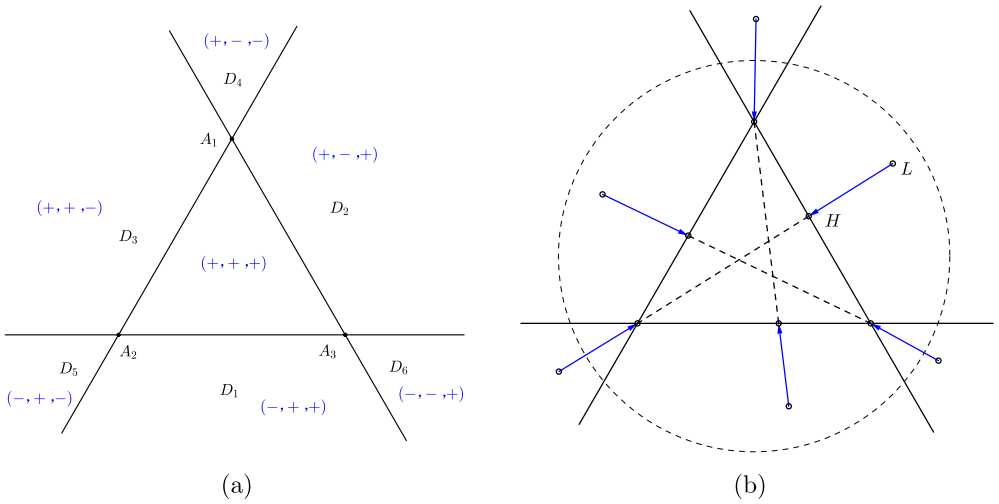

Fig. 3. Geometrical illustration of the mapping $(x_1, x_2, x_3) \mapsto (\beta_1, \beta_2, \beta_3)$.

$$\beta_i = \frac{x_i^+}{\sum_{j\in E} x_j^+}, \tag{17}$$

such that

$$\phi_i^H = \beta_i \Phi_E.$$

There is no singularity in the definition of β_i (except the fact that Φ_E may vanish, in which case we set $\phi_i^H = 0$) because

$$\sum_{j\in E} x_j^+ = \sum_{j\in E} x_j - \sum_{j\in E} x_j^- \geq \sum_{j\in E} x_j = 1.$$

However, after performing the nonlinear limiter above, it has not been completely successful to construct monotonicity preserving high-order RD schemes from low-order ones, except for the N scheme. The related topic has been widely discussed in [35,27]. In general, two problems would occur: the wiggle behavior of the solution and the lack of convergence. The imperfect performance of the Lax-Friedrichs scheme is not caused by an instability because the scheme is perfectly stable in L^∞ norm. There exist some methods to cure the problems, and one simple and effective way is to add some stabilizing/filtering terms to the residuals.

Following the idea in [35,27], a streamline dissipation term R_i^E can be added to the high-order residuals $\beta_i \Phi_E$, that is,

$$\phi_i^* = \beta_i \Phi_E + \Theta_E h_E R_i^E, \quad R_i^E = \int_E \left(\boldsymbol{\Omega}\cdot\nabla\psi_i\right)\tau\left(\boldsymbol{\Omega}\cdot\nabla I_h\right)\mathrm{d}\boldsymbol{r},$$

where $\tau > 0$, Θ_E is a switch parameter to scale the streamline dissipation term.

Note adding the filtering term does not destroy the conservation property (9) since $\sum_{i\in E} R_i^E = 0$ on each element, but it spoils the monotonicity preserving property of the RD scheme formally. However, in practice, the limited Lax-Friedrichs scheme with a filtering term performs quite well in numerical simulations, which is referred to as an essentially non-oscillatory RD scheme [35].

3.4. Second-order RD scheme

Let us go back to the steady RTE (7), and the remaining task is to distribute the residual arising from the source term S. We split the total element residual into two parts

$$\Phi_E = \int_E \boldsymbol{\Omega}\cdot\nabla I_h \mathrm{d}\boldsymbol{r} - \int_E S_h(I_h)\mathrm{d}\boldsymbol{r} = \Phi_E^a - \Phi_E^s,$$

where Φ_E^a and Φ_E^s denote the element residual associated with the advection term and general source term S, respectively.

We have represented the distribution strategy for the advection element residual Φ_E^a in Section 3.3, which is monotonicity preserving high-order accurate. We would like to split the source element residual Φ_E^s in a consistent way, while maintaining the good property of distribution methods of advection element residual.

To achieve this target, we consider the equivalent variational formulation of RD method. To be more specific, if we have already known the strategy of advection element residual, i.e.

$$\phi_i^{E,a} = \beta_i^E \Phi_E^a,$$

where the distribution coefficients β_i^E are known. Assume we find a Petrov-Galerkin test function v_i such that on every element E

$$\phi_i^{E,a} = \int_E v_i(\boldsymbol{\Omega} \cdot \nabla I_h) \mathrm{d}\boldsymbol{r} = \beta_i^E \Phi_E^a, \tag{18}$$

which satisfies

$$\sum_{i \in E} v_i = 1.$$

In general, the choice of $v_i(\boldsymbol{r})$ would not be unique. In the case of P^1 element, there are different forms of possible test function v_i, such as

$$v_i|_E = \beta_i^E \chi_E, \quad \text{or} \quad v_i|_E = \psi_i + (\beta_i^E - \frac{1}{3}),$$

where χ_E denotes the characteristic function

$$\chi_E(\boldsymbol{r}) = \begin{cases} 1, & \text{if } \boldsymbol{r} \in E, \\ 0, & \text{otherwise.} \end{cases}$$

We could readily verify the test functions v_i satisfy the condition (18).

Once we determine a test function v_i, we can cope with the source element residual consistently, that is,

$$\phi_i^E = \int_E v_i \big(\boldsymbol{\Omega} \cdot \nabla I_h - S_h(I_h)\big) \mathrm{d}\boldsymbol{r} = \beta_i^E \Phi_E^a - \int_E v_i S_h(I_h) \mathrm{d}\boldsymbol{r}. \tag{19}$$

Here we would adopt the test function $v_i = \beta_i^E \chi_E$ for constructing a second-order RD scheme, which is an extension of RD method for the RTE. Moreover, because β_i^Es are uniformly bounded, see the definition (17), provided that we set $v_i = \beta_i^E \chi_E$, we have the estimate

$$|\phi_i^E| = \left| \beta_i^E \int_E \big(\boldsymbol{\Omega} \cdot \nabla I_h - S_h(I_h)\big) \mathrm{d}\boldsymbol{r} \right| \le C |\Phi_E|.$$

This inequality implies that the distribution coefficient associated with (19) is always bounded. In other words, the overall RD scheme is $\mathcal{LP}$, which ensures the second-order accuracy of the scheme in the case of P^1 element.

Up till now, we have presented a complete description of spatial discretization based on RD methods for each angular discretized radiative transfer equation, and there exist some computational details that need to be further clarified.

In the pseudotime iteration formula (8), a useful time-step estimate is computed as

$$\Delta t^m = \nu \min_{i \in \mathcal{T}_h} \frac{|C_i|}{\sum_{E \ni i} \sum_{j \in E} c_{ij} + |C_i| \sigma_a}$$

for the single RTE in the discrete direction $\boldsymbol{\Omega}^m$, where $\sigma_a = \sigma_t - \sigma_s$, and ν denotes the CFL constant. We took $\nu = 0.5$ in our numerical experiments, unless otherwise specified.

When sweeping the discrete solid angles (from $m = 1$ to M) at time layer ℓ, we adopt the following strategy to compute the scattering integral term

$$I_i^{m,*} = \begin{cases} I_i^{m,(\ell)}, & \text{if it is available,} \\ I_i^{m,(\ell-1)}, & \text{otherwise,} \end{cases}$$

where $I_i^{m,*} = I_h(M_i, \boldsymbol{\Omega}^m)$ at different time layers.

We would adopt the source iterative (SI) method to compute the steady solution. The SI iteration process continues until a prescribed convergence criterion is satisfied, and we take the stop criterion as $\|I^{m,(\ell)} - I^{m,(\ell-1)}\|_\infty < \varepsilon_{non}$ in the numerical experiments in Section 4.

We summarize the algorithm of the conservative RD scheme for steady RTEs in the following Algorithm 1.

Algorithm 1 The conservative RD scheme for steady RTEs.

Input: Choose a small positive value $\varepsilon_{non} > 0$ and set initial iteration values $I_i^{m,(0)}$ for $m = 1, \ldots, M$, and each $i \in \mathcal{T}_h$.
Output: The steady solution of I_i^m, $m = 1, \ldots, M$, $i \in \mathcal{T}_h$.

1: **for** $\ell = 1$ to *maxiter* (maximum number of iterations) **do**
2: **for** $m = 1, \ldots, M$ (scanning discrete solid angles) **do**
3: set $\mathrm{Res}_i^m = 0$ for each $i \in \mathcal{T}_h$
4: **for** each E **do**
5: evaluate quantities concerning advection residual $\Phi_E^{m,a}$, $\phi_i^{m,E,a}$ and $\beta_i^{m,E}$ with

$$\beta_i^{m,E} = \frac{\left(\frac{\phi_i^{m,E,a}}{\Phi_E^{m,a}}\right)^+}{\sum\limits_{j\in E}\left(\frac{\phi_j^{m,E,a}}{\Phi_E^{m,a}}\right)^+},$$

6: calculate the modified residual $\phi_i^{m,E,*}$ with a consistent test function v_i^m, such that

$$\phi_i^{m,E,*} = \int_E v_i^m\left(\boldsymbol{\Omega}^m \cdot \nabla I_h^m - S_h^m(I_h^m)\right)\mathrm{d}\boldsymbol{r} = \beta_i^{m,E}\Phi_E^{m,a} - \int_E v_i^m S_h^m(I_h^m)\mathrm{d}\boldsymbol{r}.$$

7: update

$$\mathrm{Res}_i^m = \mathrm{Res}_i^m + \phi_i^{m,E,*}.$$

8: **end for**
9: update the nodal solution

$$I_i^{m,(\ell)} = I_i^{m,(\ell-1)} - \frac{\Delta t}{|C_i|}\mathrm{Res}_i^m, \quad \Delta t = \min_{1\le m\le M}\Delta t^m.$$

10: **end for**
11: use

$$\|I^{m,(\ell)} - I^{m,(\ell-1)}\|_\infty \le \varepsilon_{non}$$

12: as the stop criterion.
13: **end for**

Remark 3.2. Though there exist some small differences in the implementation of overall schemes based on the N scheme and Lax-Friedrichs scheme, which are referred to as the LN scheme and LLxF scheme later, respectively, the detailed algorithm we present here can be applied to both RD schemes. The only difference is adding a filtering term to the residuals when adopting the LLxF scheme.

4. Numerical experiments

In this section, several numerical experiments are carried out to validate the accuracy and non-oscillatory property of RD schemes on unstructured meshes. Regarding the discrete-ordinate quadrature rule, we adopt the Legendre-Chebyshev P_N-T_N quadrature [41] in which the μ-levels are equal to the roots of the Gauss-Legendre quadrature, and the azimuthal angles φ are determined from the roots of the orthogonal Chebyshev polynomials. To be more specific, S_8 and P_8-T_8 quadrature sets are adopted for all the following 1D and 2D numerical tests with nonzero scattering terms, respectively, unless otherwise stated.

Example 4.1. The one-dimensional radiative transfer equation simulating the absorbing-scattering model.

We first consider the 1D steady radiative transfer equation (2) with $\sigma_t = 2200$, $\sigma_s = 1$ and $q(z,\mu) = -4\pi\mu^3\cos^3\pi z \sin\pi z + \sigma_t(\mu^2\cos^4\pi z + a) - \sigma_s(a + \frac{\cos^4\pi z}{3})$. Here $a = 10^{-14}$ is a small positive constant. This problem is a smooth numerical test in [7], which aims to verify the accuracy of the schemes. The computational domain is $\mathbb{D} = [0, 1]$. The boundary conditions are given by

$$\begin{cases} I(0,\mu) = \mu^2 + a, & \text{if } \mu > 0, \\ I(1,\mu) = \mu^2 + a, & \text{if } \mu < 0. \end{cases}$$

The exact solution is given by $I(z,\mu) = \mu^2\cos^4\pi z + a$.

We adopt the LLxF scheme to solve the 1D steady absorbing-scattering problem. The numerical errors of the LLxF scheme are shown in Table 1. It can be seen clearly that the second-order convergence rates are achieved in different discrete norms. Fig. 4(a) displays the numerical solution using the LLxF scheme on an 80 uniform grid in different discrete directions

Table 1
Errors and convergence orders of the LLxF RD scheme for the 1D RTE.

h	L^1-error	Order	L^2-error	Order	L^∞-error	Order
1/20	2.263E-3	–	2.620E-3	–	5.211E-3	–
1/40	3.862E-4	2.551	4.875E-4	2.426	1.322E-3	1.979
1/80	7.425E-5	2.379	9.707E-5	2.328	3.243E-4	2.027
1/160	1.785E-5	2.056	2.222E-5	2.127	7.729E-5	2.069
1/320	4.445E-6	2.006	5.415E-6	2.037	1.765E-5	2.131
1/640	1.111E-6	2.000	1.347E-6	2.007	3.777E-6	2.224

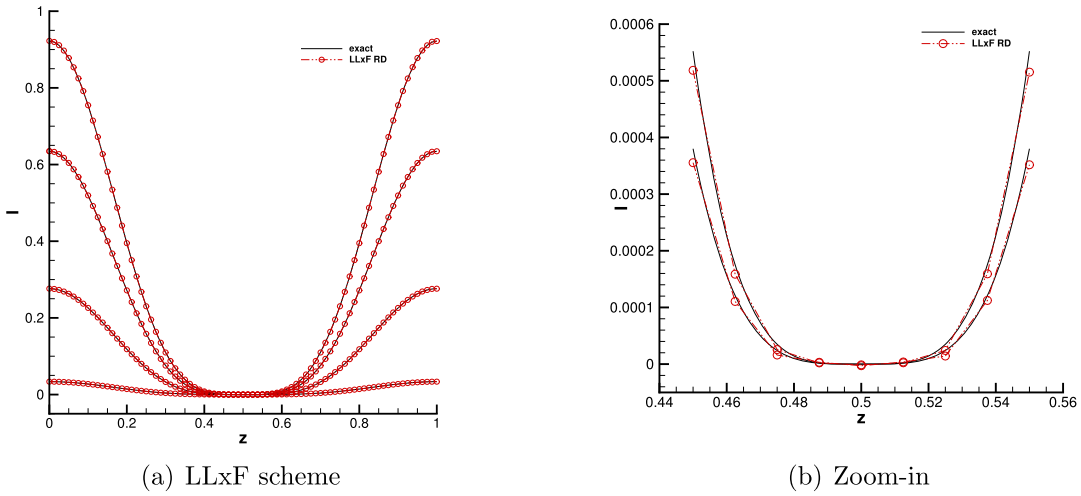

(a) LLxF scheme (b) Zoom-in

Fig. 4. The comparison of exact and numerical solutions for the 1D RTE on an 80 uniform grid in directions (a) $\mu = [-0.9603, -0.7967, -0.5255, -0.1834]$ (from top to bottom) and (b) $\mu = [-0.9603, -0.7967]$ (from top to bottom).

$\mu = [-0.9603, -0.7967, -0.5255, -0.1834]$ from top to bottom, respectively. The plots are omitted in the remaining four directions due to the symmetry with respect to μ of the solution. We also provide a zoom-in figure of the solution on the same mesh in the directions $\mu = -0.9603$ (top) and $\mu = -0.7967$ (bottom), respectively, which is shown in Fig. 4(b). We observe that the numerical solution matches very well with the exact solution.

Example 4.2. The two-dimensional smooth radiative transfer equation.

We consider the 2D steady radiative transfer equation (3) in [7] with $\sigma_t = 1$, $\sigma_s = 0$ and source function $q = 0$ on a square $\mathbb{D} = [0, 1] \times [0, 1]$. Here we set $\zeta = 0.5$, $\eta = 0.1$. The boundary conditions are set as

$$I(x, 0, \zeta, \eta) = 0, \quad I(0, y, \zeta, \eta) = \sin^6(\pi y).$$

The exact solution is given as follows

$$I(x, y, \zeta, \eta) = \begin{cases} 0, & y < \frac{\eta}{\zeta} x, \\ \sin^6\left(\pi (y - \frac{\eta}{\zeta} x)\right) e^{-\frac{\sigma_t}{\zeta} x}, & \text{otherwise}. \end{cases} \tag{20}$$

The analytic solution to this model problem is smooth, which is adopted to test the accuracy of our proposed scheme. We adopt the LN scheme to simulate the solution on unstructured triangular meshes. Table 2 displays the numerical errors on a set of successively refined meshes, which shows that second-order convergence rates are achieved in different discrete norms.

Example 4.3. The two-dimensional radiative transfer equation simulating the transparent model.

In this test, we consider the 2D steady radiative transfer equation simulating the transparent model, with $\sigma_t = 0$, $\sigma_s = 0$, and source function $q = 0$. The computational domain is $\mathbb{D} = [0, 1] \times [0, 1]$. Here we set the direction $\zeta = 0.7$, $\eta = 0.7$. The boundary conditions are

$$I(x, 0, \zeta, \eta) = 0, \quad I(0, y, \zeta, \eta) = 1.$$

Table 2
Errors and convergence orders of the LN RD scheme for the 2D RTE.

h	L^1-error	Order	L^2-error	Order	L^∞-error	Order
1.017E-1	3.522E-3	–	5.318E-3	–	1.752E-2	–
5.087E-2	1.094E-3	1.687	1.572E-3	1.758	5.555E-3	1.657
2.543E-2	2.655E-4	2.042	3.815E-4	2.043	1.539E-3	1.852
1.272E-2	6.503E-5	2.029	9.318E-5	2.034	4.046E-4	1.928
6.359E-3	1.652E-5	1.977	2.316E-5	2.008	9.754E-5	2.053

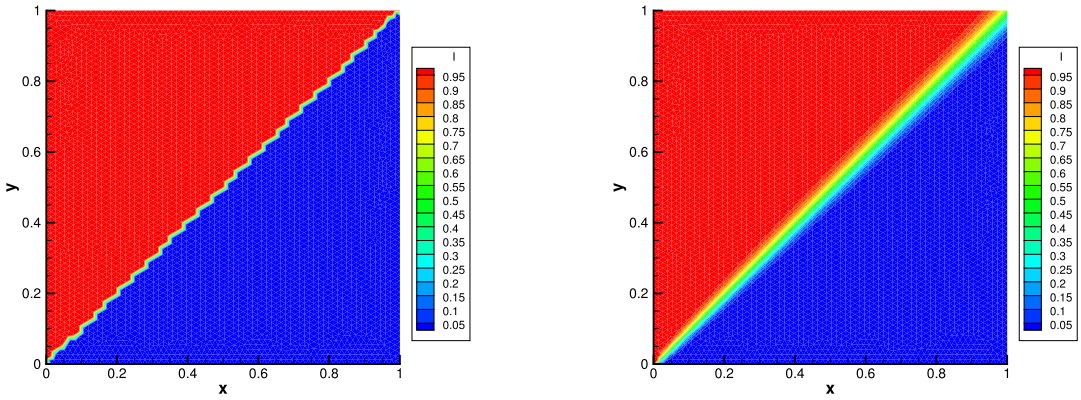

(a) Exact (b) LN scheme

Fig. 5. Isolines of the exact and numerical solutions for the 2D RTE simulating the transparent model.

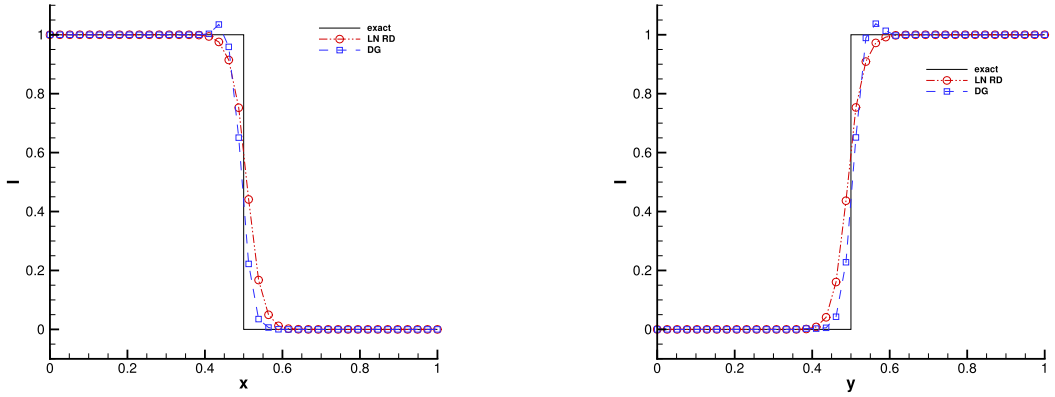

(a) Cross-section along $y = 0.5$ (b) Cross-section along $x = 0.5$

Fig. 6. The comparison of the radiative intensity cut along (a) $y = 0.5$ and (b) $x = 0.5$ with 40 sample points for the 2D RTE simulating the transparent model.

The exact solution is given as follows

$$I(x, y, \zeta, \eta) = \begin{cases} 0, & y < \frac{\eta}{\zeta} x, \\ 1, & \text{otherwise}. \end{cases}$$

We choose this model problem to validate the non-oscillatory property of the LN scheme since there exists a discontinuity along the line $y = x$. Fig. 5 shows isolines of the exact and numerical solutions on the unstructured triangular mesh with mesh size $h = 2.015E-2$ (9820 elements, 5041 vertices). We display cross sections of numerical solutions along the line $y = 0.5$ and $x = 0.5$ with 40 sample points in Fig. 6. We also plot the numerical solution simulated by the P^1 DG scheme with the scaling positivity-preserving limiter in [8]. In the comparison of numerical solutions, we observe the numerical solution by the LN RD scheme has no undershoot and overshoot problem across the discontinuity. Moreover, the number of DoFs on the same computational mesh for the RD scheme is greatly less than that for the DG scheme, since the RD scheme

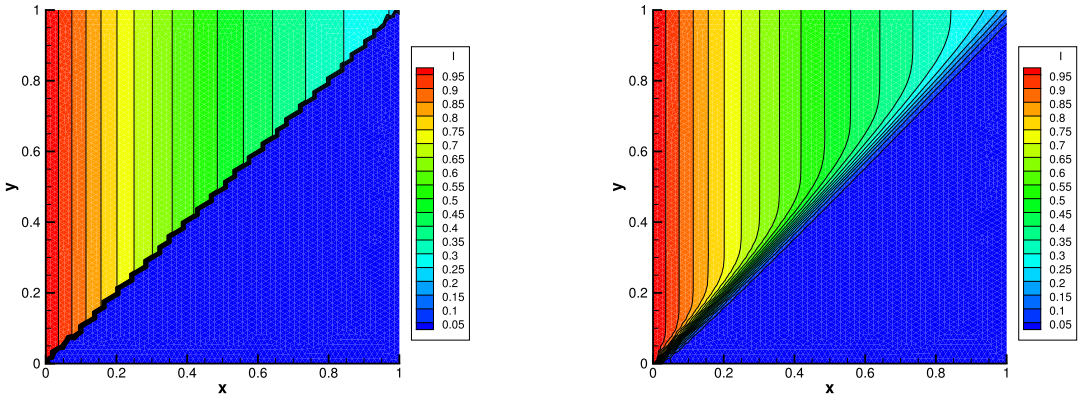

(a) Exact (b) LN scheme

Fig. 7. Isolines of the exact and numerical solutions for the 2D RTE simulating the purely absorbing model.

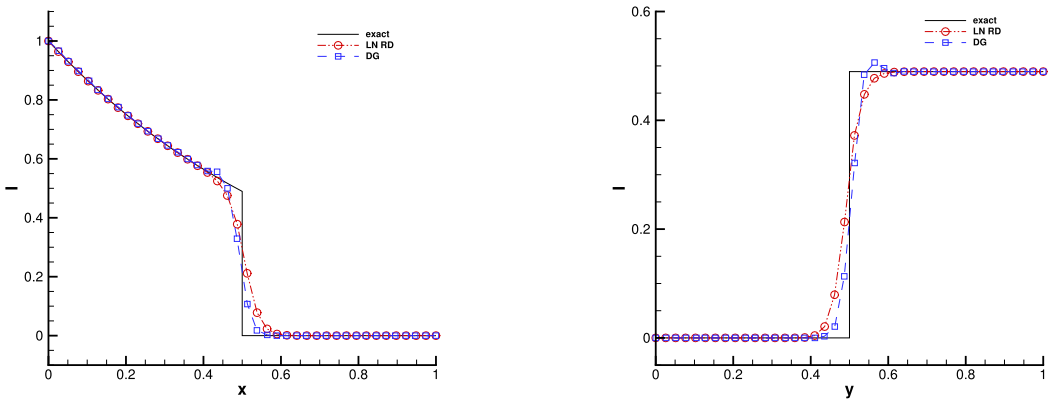

(a) Cross-section along $y = 0.5$ (b) Cross-section along $x = 0.5$

Fig. 8. The comparison of the radiative intensity cut along (a) $y = 0.5$ and (b) $x = 0.5$ with 40 sample points for the 2D RTE simulating the purely absorbing model.

adopts the continuous finite element spaces, refer to [27]. This example validates the non-oscillatory property of the RD scheme.

Example 4.4. The two-dimensional radiative transfer equation simulating the purely absorbing model.

In this test, we consider the 2D steady radiative transfer equation simulating the purely absorbing model in [7], with $\sigma_t = 1$, $\sigma_s = 0$ and $q = 0$. The computational domain is $\mathbb{D} = [0, 1] \times [0, 1]$. We consider the direction $\zeta = 0.7$, $\eta = 0.7$. The boundary conditions are

$$I(x, 0, \zeta, \eta) = 0, \quad I(0, y, \zeta, \eta) = 1.$$

The exact solution is given as follows

$$I(x, y, \zeta, \eta) = \begin{cases} 0, & y < \frac{\eta}{\zeta} x, \\ e^{-\frac{\sigma_t}{\zeta} x}, & \text{otherwise}. \end{cases}$$

This problem can be seen as a variant version of the previous problem in Example 4.3. Here we adopt the LN scheme to simulate the solution on unstructured triangular meshes. We display isolines of the exact and numerical solutions on the mesh with $h = 2.015E - 2$, from which we observe a good performance of the numerical solution. It can be seen that isolines above the line $y = x$ are straight, see Fig. 7. Fig. 8 displays the comparison of the radiative intensity simulated by the LN RD scheme and P^1 DG scheme with the scaling positivity-preserving limiter, along the line $y = 0.5$ and $x = 0.5$, respectively. We also observe that there is no undershoot and overshoot problem across the discontinuity in our numerical

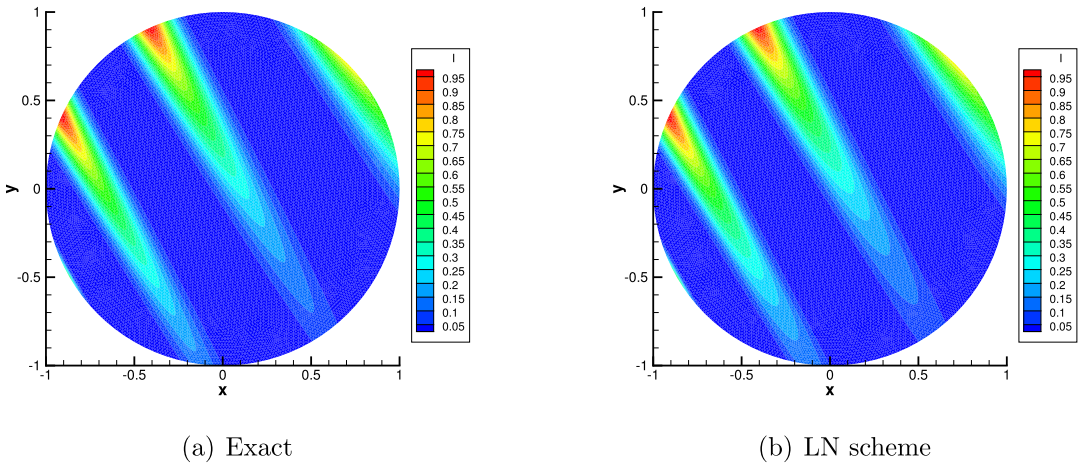

Fig. 9. Isolines of the exact and numerical solutions for the 2D RTE simulating the absorbing model on a circular domain.

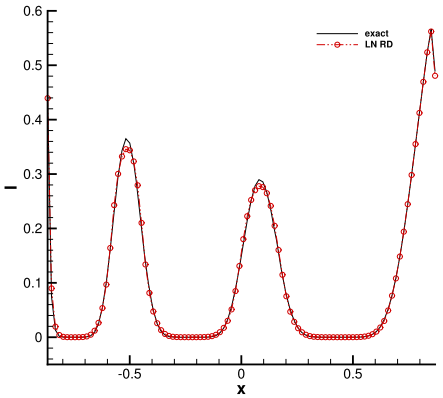

Fig. 10. Plot of the solutions cut along the line $y = \frac{4}{7}x$ with 100 sample points for the 2D RTE simulating the absorbing model on a circular domain.

solution. It shows the good quality of the proposed RD scheme which has used fewer DoFs compared to the DG scheme on the same mesh.

Example 4.5. The two-dimensional radiative transfer equation simulating the absorbing model on a circular domain.

We consider the 2D steady radiative transfer equation (3) on a circular domain in [8], with $\sigma_t = 1$, $\sigma_s = 0$ and source function $q = 0$. The computational domain is $\mathbb{D} = \{(x, y) |\ x^2 + y^2 \leq 1\}$. Here we set $\zeta = 0.4$, $\eta = -0.7$. The boundary conditions are

$$I(x, y, \zeta, \eta) = \sin^8\left(\pi(x + y)\right), \quad (x, y) \in \partial\mathbb{D}_{\text{in}}.$$

For this problem, we have the exact solution as

$$I(x, y, \zeta, \eta) = \sin^8\left(\pi(x + y - (\zeta + \eta)\xi)\right)\mathrm{e}^{-\sigma_t \xi},$$

where $\xi = \left(\zeta x + \eta y + \sqrt{\zeta^2 + \eta^2 - (\eta x - \zeta y)^2}\right)/(\zeta^2 + \eta^2)$.

We solve the problem on an unstructured triangular mesh with mesh size $h = 2.15E - 2$ (totally 27936 elements). Fig. 9 plots the isolines of the exact solution and numerical solution using the LN scheme respectively. Fig. 10 shows the cross section of solutions along the line $y = -\frac{\zeta}{\eta}x$, in which we use 100 sample points. We find our numerical result matches well with the exact solution, even at these extreme points.

Example 4.6. The two-dimensional radiative transfer equation simulating the absorbing-scattering model.

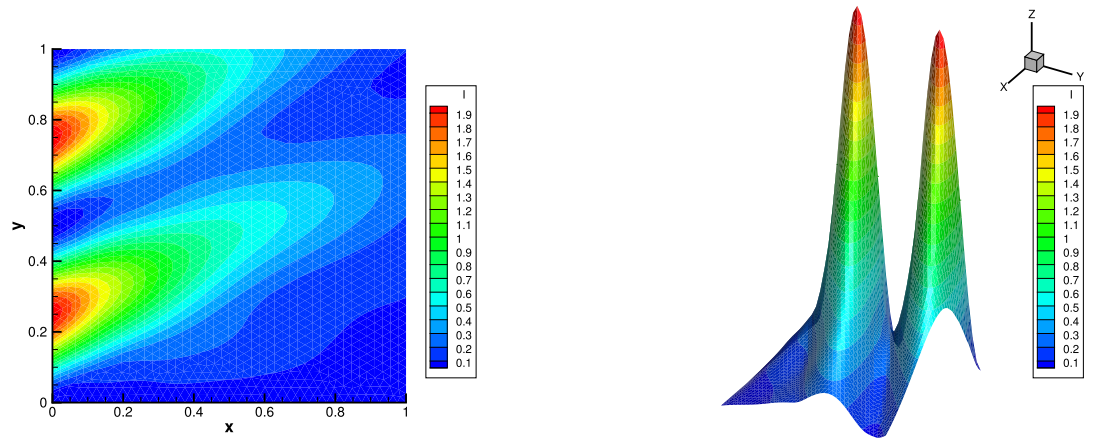

Fig. 11. Isoline (left) and profile (right) of the numerical solution in $\mathbf{\Omega} = (0.2578, 0.1068)$ for the 2D RTE simulating the absorbing-scattering model.

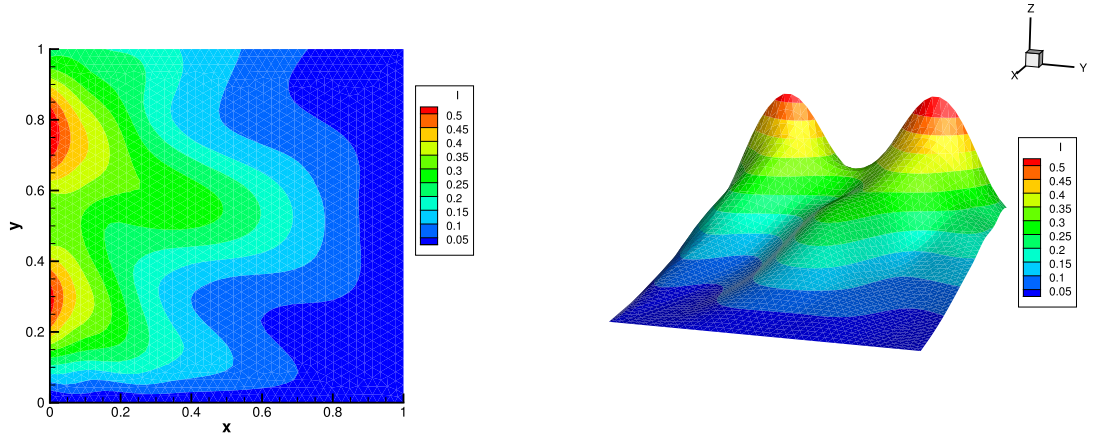

Fig. 12. Isoline (left) and profile (right) of the numerical solution in $\mathbf{\Omega} = (-0.2578, 0.1068)$ for the 2D RTE simulating the absorbing-scattering model.

In this problem, we test the conservative RD scheme on the 2D RTE simulating the absorbing-scattering model in [7], with $\sigma_t = 1$, $\sigma_s = 1$ and $q = 0$. The computational domain is $\mathbb{D} = [0, 1] \times [0, 1]$. The boundary conditions are set on each edge of the square

$$I(x, 0, \zeta, \eta) = 0, \quad \eta > 0; \; I(x, 1, \zeta, \eta) = 0, \quad \eta < 0;$$
$$I(0, y, \zeta, \eta) = 1 - \cos(4\pi y), \quad \zeta > 0; \; I(1, y, \zeta, \eta) = 0, \quad \zeta < 0.$$

For this problem, we have no explicit analytical solution. We adopt the LN scheme to simulate the solution on unstructured mesh with $h = 2.96E - 2$ (with 3702 elements). Fig. 11 displays the isoline and profile of the numerical result in the direction $\mathbf{\Omega} = (0.2578, 0.1068)$. Fig. 12 displays the isoline and profile of the numerical result in the direction $\mathbf{\Omega} = (-0.2578, 0.1068)$. We can observe that there are no undershoots and overshoots in the numerical results. The results also indicate the effectiveness of our schemes.

5. Conclusion

In this paper, conservative residual distribution methods on unstructured meshes have been developed for the numerical solution of steady radiative transfer equations. We adopt the discrete ordinate method for the discretization of angular space, then use the RD method to solve the resulting system of linear hyperbolic equations. We recall the basic formulations and design principles of RD methods, then give the accuracy analysis of RD schemes. We use the standard technique to upgrade the accuracy of monotonicity preserving RD scheme, then discretize the absorbing-scattering and source term consistently based on the variational formulation. The proposed RD schemes inherit the advantages of the classical ones. Numerical results on a wide number of steady RTEs show the good accuracy and non-oscillatory property of our RD schemes. Considering the complexity of radiative transfer, we consider a relatively simple one-group model for designing the numerical

schemes here, while the efficient numerical simulation of multi-group RTEs is a quite challenging task. The extension to higher-order RD schemes for unsteady RTEs would be considered in our next work.

CRediT authorship contribution statement

Jiexing Zhang: Conceptualization, Methodology, Software, Data curation, Writing – Original draft preparation. **Qingjie Cui**: Visualization, Investigation, Writing – Reviewing and Editing. **Yinbing Chen**: Vice-Supervision **Guoxi Ni**: Supervision.

Declaration of competing interest

The authors declare that they have no known competing financial interests or personal relationships that could have appeared to influence the work reported in this paper.

Data availability

Data will be made available on request.

Acknowledgement

The authors are supported by National Key R&D Program of China 2022YFA1004500, NSFC (Nos. 12171049, 12292982, 11771055, 11871113, 11871114, 11671050, 12026607) and 3D numerical simulation platform TB14-1 of China academy of engineering physics.

References

[1] J.R. Howell, M. Perlmutter, Monte Carlo solution of thermal transfer through radiant media between gray walls, J. Heat Transf. 86 (1964) 116–122.
[2] J.T. Farmer, J.R. Howell, Monte Carlo prediction of radiative heat transfer in inhomogeneous, anisotropic, nongray media, J. Thermophys. Heat Transf. 8 (1994) 133–139.
[3] M.P. Mengüç, R.K. Iyer, Modeling of radiative transfer using multiple spherical harmonics approximations, J. Quant. Spectrosc. Radiat. Transf. 39 (1988) 445–461.
[4] S. Chandrasekhar, Radiative Transfer, Clarendon Press, Oxford, 1950.
[5] G.D. Raithby, E.H. Chui, A finite-volume method for predicting a radiant heat transfer in enclosures with participating media, J. Heat Transf. 112 (1990) 415–423.
[6] M.M. Razzaque, D.E. Klein, J.R. Howell, Finite element solution of radiative heat transfer in a two-dimensional rectangular enclosure with gray participating media, J. Heat Transf. 105 (1983) 933–936.
[7] D. Yuan, J. Cheng, C.-W. Shu, High order positivity-preserving discontinuous Galerkin methods for radiative transfer equations, SIAM J. Sci. Comput. 38 (2016) A2987–A3019.
[8] M. Zhang, J. Cheng, J. Qiu, High order positivity-preserving discontinuous Galerkin schemes for radiative transfer equations on triangular meshes, J. Comput. Phys. 397 (2019) 108811.
[9] M. Zhang, W. Huang, J. Qiu, High-order conservative positivity-preserving DG-interpolation for deforming meshes and application to moving mesh DG simulation of radiative transfer, SIAM J. Sci. Comput. 42 (2020) A3109–A3135.
[10] J.M. Zhao, L.H. Liu, Least-squares spectral element method for radiative heat transfer in semitransparent media, Numer. Heat Transf., Part B, Fundam. 50 (2006) 473–489.
[11] W. Sun, S. Jiang, K. Xu, An asymptotic preserving unified gas kinetic scheme for gray radiative transfer equations, J. Comput. Phys. 285 (2015) 265–279.
[12] W. Sun, S. Jiang, K. Xu, A multidimensional unified gas-kinetic scheme for radiative transfer equations on unstructured mesh, J. Comput. Phys. 351 (2017) 455–472.
[13] S. Tan, W. Sun, K. Xu, J. Wei, G. Ni, Time implicit unified gas kinetic scheme for 3D multi-group neutron transport simulation, Commun. Comput. Phys. 28 (2020) 1189–1218.
[14] M.F. Modest, Radiative Heat Transfer, Academic press, 2013.
[15] R.-H. Ni, A multiple grid scheme for solving the Euler equations, AIAA J. 20 (1982) 1565–1571.
[16] P.L. Roe, Fluctuations and signals—a framework for numerical evolution problems, Numer. Methods Fluid Dyn. (1982) 219–257.
[17] S.M.J. Guzik, C.P.T. Groth, Comparison of solution accuracy of multidimensional residual distribution and Godunov-type finite-volume methods, Int. J. Comput. Fluid Dyn. 22 (2008) 61–83.
[18] R. Abgrall, Toward the ultimate conservative scheme: following the quest, J. Comput. Phys. 167 (2001) 277–315.
[19] R. Abgrall, M. Mezine, Construction of second order accurate monotone and stable residual distribution schemes for unsteady flow problems, J. Comput. Phys. 188 (2003) 16–55.
[20] M. Ricchiuto, Á. Csík, H. Deconinck, Residual distribution for general time-dependent conservation laws, J. Comput. Phys. 209 (2005) 249–289.
[21] R. Abgrall, D.D. Santis, M. Ricchiuto, High-order preserving residual distribution schemes for advection-diffusion scalar problems on arbitrary grids, SIAM J. Sci. Comput. 36 (2014) A955–A983.
[22] N. Villedieu, T. Quintino, M. Ricchiuto, H. Deconinck, Third order residual distribution schemes for the Navier–Stokes equations, J. Comput. Phys. 230 (2011) 4301–4315.
[23] R. Abgrall, D.D. Santis, Linear and non-linear high order accurate residual distribution schemes for the discretization of the steady compressible Navier–Stokes equations, J. Comput. Phys. 283 (2015) 329–359.
[24] M. Ricchiuto, R. Abgrall, H. Deconinck, Application of conservative residual distribution schemes to the solution of the shallow water equations on unstructured meshes, J. Comput. Phys. 222 (2007) 287–331.
[25] M. Ricchiuto, An explicit residual based approach for shallow water flows, J. Comput. Phys. 280 (2015) 306–344.
[26] R. Abgrall, P.L. Roe, High order fluctuation schemes on triangular meshes, J. Sci. Comput. 19 (2003) 3–36.
[27] R. Abgrall, A. Larat, M. Ricchiuto, Construction of very high order residual distribution schemes for steady inviscid flow problems on hybrid unstructured meshes, J. Comput. Phys. 230 (2011) 4103–4136.

[28] J. Lin, Y. Ren, R. Abgrall, J. Qiu, High order residual distribution conservative finite difference HWENO scheme for steady state problems, J. Comput. Phys. 457 (2022) 111045.
[29] R. Abgrall, High order schemes for hyperbolic problems using globally continuous approximation and avoiding mass matrices, J. Sci. Comput. 73 (2017) 461–494.
[30] R. Abgrall, P. Bacigaluppi, S. Tokareva, High-order residual distribution scheme for the time-dependent Euler equations of fluid dynamics, Comput. Math. Appl. 78 (2019) 274–297.
[31] L. Arpaia, M. Ricchiuto, Well balanced residual distribution for the ALE spherical shallow water equations on moving adaptive meshes, J. Comput. Phys. 405 (2020) 109173.
[32] R. Abgrall, D. Torlo, High order asymptotic preserving deferred correction implicit-explicit schemes for kinetic models, SIAM J. Sci. Comput. 42 (2020) B816–B845.
[33] R. Abgrall, M. Ricchiuto, Hyperbolic balance laws: residual distribution, local and global fluxes, in: Numerical Fluid Dynamics, 2022, pp. 177–222.
[34] R. Struijs, H. Deconinck, P.L. Roe, Fluctuation splitting schemes for the 2D Euler equations, in: Computational Fluid Dynamics, VKI LS 1991-01, 1991.
[35] R. Abgrall, Essentially non-oscillatory residual distribution schemes for hyperbolic problems, J. Comput. Phys. 214 (2006) 773–808.
[36] J.-L. Guermond, M. Nazarov, B. Popov, Y. Yang, A second-order maximum principle preserving Lagrange finite element technique for nonlinear scalar conservation equations, SIAM J. Numer. Anal. 52 (2014) 2163–2182.
[37] D. Kuzmin, M.Q. de Luna, Algebraic entropy fixes and convex limiting for continuous finite element discretizations of scalar hyperbolic conservation laws, Comput. Methods Appl. Mech. Eng. 372 (2020) 113370.
[38] H. Hajduk, D. Kuzmin, T. Kolev, V. Tomov, I. Tomas, J.N. Shadid, Matrix-free subcell residual distribution for Bernstein finite elements: monolithic limiting, Comput. Fluids 200 (2020) 104451.
[39] G.C. Pomraning, The Equations of Radiation Hydrodynamics, 1973.
[40] H. Deconinck, M. Ricchiuto, Residual distribution schemes: foundations and analysis, in: Encyclopedia of Computational Mechanics, second edition, 2018, pp. 1–53.
[41] K.D. Lathrop, B.G. Carlson, Discrete ordinates angular quadrature of the neutron transport equation, Tech. Report LA-3186, Los Alamos Scientific Laboratory, 1964.